FINAL TECHNICAL REPORT

AWARD #**DE-FC26-07NT43228**
TITLE: **"HIGH-EFFICIENCY NON-POLAR GaN-BASED LEDs"**

RECIPIENT: INLUSTRA TECHNOLOGIES, LLC
Principle Investigator: Paul T. Fini, Inlustra Technologies
Subcontractor: Univ. of California, Santa Barbara
DoE Project Officer: Brian Dotson
Period: 9/1/07 – 12/31/08 (incl. NCE)

DISCLAIMER

EXECUTIVE SUMMARY

Inlustra Technologies with subcontractor U.C. Santa Barbara conducted a project with the principle goal of demonstrating high internal quantum efficiency blue (430 nm) and green (540nm) light emitting diodes (LEDs) on low-defect density non-polar GaN wafers.

Inlustra pursued the fabrication of smooth thick *a*-plane and *m*-plane GaN films, as well as defect reduction techniques such as lateral epitaxial overgrowth (LEO) to uniformly lower dislocation density in these films. Limited free-standing wafers were produced as well. By the end of the reporting period, Inlustra had met its milestone of dislocation reduction to $< 5 \times 10^6$ cm^{-2}. Stacking faults were still present in appreciable density ($\sim 1 \times 10^5$ cm^{-1}), but were not the primary focus of defect reduction since there have been no published studies establishing their detrimental effects on LED performance. Inlustra's LEO progress built a solid foundation upon which further commercial development of GaN substrates will occur.

UCSB encountered multiple delays in its LED growth and fabrication efforts due to unavoidable facilities outages imposed by ongoing construction in an area adjacent to the metalorganic chemical vapor deposition (MOCVD) laboratory. This, combined with the large amount of *ab initio* optimization required for the MOCVD system used during the project, resulted in unsatisfactory LED progress. Although numerous blue-green photoluminescence results were obtained, only a few LED structures exhibited electroluminescence at appreciable levels.

UCSB also conducting extensive modelling (led by Prof. Van de Walle) on the problem of non-radiative Auger recombination in GaN-based LED structures, which has been posited to contribute to LED efficiency 'droop' at elevated current density. Unlike previous modelling efforts, UCSB's approach was truly a first-principles *ab initio* methodology. Building on solid numerical foundations, the Auger recombination rates of $In_xGa_{1-x}N$ alloys were calculated from first-principles density-functional and many-body-perturbation theory. The differing mechanisms of inter- and intra-band recombination were found to affect different parts of the emission spectrum. In the blue to green spectral region and at room temperature the Auger coefficient was calculated to be as large as 2×10^{-30} cm^6 s^{-1}; in the infrared it is even larger. These results indicated that Auger recombination may be responsible for the loss of quantum efficiency that affects InGaN-based light emitters, whether on non-polar or polar crystal planes.

ACCOMPLISHMENT OF PROJECT GOALS

Below is a summary of Project Milestones (as approved in the Management Plan) and the progress reached toward each. There were significant delays in negotiating and finalizing the subcontract with UCSB, such that the sub-award did not officially start until early in 2008. In addition, delays in hiring post-doctoral researchers were encountered. Finally, adequate allocation of MOCVD growth system time at UCSB did not occur until ten months into the project, due to numerous lab-wide outages related to facilities upgrades. All of these issues led to unsatisfactory LED growth and fabrication progress at UCSB.

1. YEAR 1 MILESTONES

Milestone Title: **Growth optimization for blue (430-450 nm) and green (540 nm) non-polar InGaN quantum wells**
Planned Completion Date: **9/30/08**
Description & Verification Method:
UCSB will conduct initial MOCVD growth optimization of non-polar LED active regions, with primary focus on InGaN quantum well growth parameters, especially for green (540 nm) emission. p-type GaN layer development will be a secondary, but important, focus of initial MOCVD growth optimization. Most first-year growth studies will be carried out on defective GaN template films, grown by MOCVD or MBE (UCSB) or HVPE (Inlustra). Blue (430-450 nm) LED active region development will be performed on *a*-plane or *m*-plane GaN templates, while green LED development will be confined to *m*-plane GaN templates. The packaged LED output goal for both orientations will be a minimum of 2 mW at a current density 22 A/cm^2. We note here that if *a*-plane blue LEDs of sufficient output power cannot be fabricated, or if the desired wavelength range (430-450 nm) cannot be reproducibly reached, further development of *a*-plane LEDs will cease. Instead, *m*-plane films will be used for both blue and green LED development.

Progress Toward Milestone:
As mentioned above, the least satisfactory aspect of the project was the growth and fabrication of blue and green non-polar LEDs by UCSB. Between personnel and facilities delays, significant progress in LED film growth was not made until late in the project. LED film growth optimization did not proceed as far as expected, so that although some promising blue-green quantum well photoluminescence (PL) results were obtained, satisfactory electroluminescence (EL, *i.e.* light production via electrical current flow) was not achieved. Much of the growth development had to be started from scratch, since the MOCVD system had not been utilized for LED growth in several years. InGaN quantum well growth conditions in particular were difficult to optimize in the time allotted.

Milestone Title: **Initial development of direct LED Internal Quantum Efficiency (IQE) measurement technique**
Planned Completion Date: **9/30/08**
Description & Verification Method:

Initial development of the LED internal quantum efficiency (IQE) measurement technique will focus on establishing a geometric and mathematical basis for self-consistent measurements. UCSB personnel will design photolithographic masks with a variety of features for establishing standard measurement approaches on different types of samples. The first IQE measurements under current injection will be carried out on well-characterized LED structures, such that correlations may be made with output power as measured by a calibrated integrating sphere. Angular-resolved measurements will be employed to validate light extraction calculations. In addition, results will be compared to calibrated low- and room-temperature photoluminescence measurements on the quantum well active regions of the LEDs.

Progress Toward Milestone:

At its own expense, UCSB performed initial work on the measurement of LED structure IQE via electrically-pumped luminescence measurements. The principle focus was development of a highly absorbing mask material that would allow the controlled and predictable collection of light from apertures of various sizes. Given a high enough absorption, this mask (and sidewall coating) should minimize multiple internal reflections that would complicate correlation of light output power to electrical input power. Rigorous modelling of light production and collection using dipole emission and a scattering matrix formalism revealed that absorption of the coating was sufficient for the purposes of initially studying light emission vs. aperture size (*i.e.* escape angle). LED film surface roughness was also taken into account as a factor that can unintentionally increase light extraction efficiency, and therefore the apparent IQE that is measured.

Milestone Title: **Fully coalesced, planar *a*-plane and *m*-plane GaN HVPE LEO**
Planned Completion Date: **9/30/08**
Description & Verification Method:
Inlustra will expand on initial lateral epitaxial overgrowth (LEO) methodology developed at UCSB to produce high-quality non-polar GaN templates for device development. The primary objectives will be to achieve uniformly low threading dislocation ($< 5 \times 10^6$ cm^{-2}) and stacking fault densities over full two-inch wafers. Hydride vapor phase epitaxy (HVPE) growth parameters will be refined to minimize stacking fault generation and facilitate smooth coalescence of LEO stripes. If smooth, coalesced films cannot be achieved by this approach, lapping and polishing may be employed to provide suitable surfaces for device re-growth. Atomic force microscopy (AFM) and transmission electron microscopy (TEM) will be employed to confirm that the film surfaces have uniformly low threading dislocation and stacking fault densities.

Progress Toward Milestone:

Inlustra first refined its HVPE growth conditions for heteroepitaxial non-polar a- and m-plane GaN films by focusing on obtaining smooth surface morphology regardless of dislocation density. Most studies were conducted on *a*-plane films, though smooth *m*-plane films were also pursued. In cases when an as-grown film was insufficiently smooth for subsequent LEO patterning, lapping and polishing was applied in house. LEO of two different variants was then performed, using either 'standard' stripe patterning in SiO_2 masks, or 'Sidewall' LEO, which involved SiO_2 patterning followed by dry etching of the underlying GaN film to form periodic trenches. Re-growth experiments then determined optimal stripe period spacing (***e.g.*** 15μm vs. 35μm of mask between openings), as well as refinement of HVPE growth conditions to obtain smooth coalescence between neighboring stripes. The result was uniform dislocation density reduction to average levels $< 5 \times 10^6$ cm^{-2}, though in some cases stacking faults remained at a density of $\sim 1 \times 10^5$ cm^{-1}. The effect of stacking faults on device performance is unknown, but there were indications in UCSB's LED film growth studies that they can induce surface roughness under various MOCVD growth conditions.

Milestone Title: **Determination of key parameters for LED simulations**
Planned Completion Date: **9/30/08**
Description & Verification Method:
UCSB researchers will determine key parameters such as band offsets and deformation potentials to enable accurate modeling of the energy band diagrams for equivalent polar and non-polar (Al,In)GaN multi-layer LED structures. Such parameters, where necessary, may need to be evaluated in equilibrium as well as under current injection of various levels. Previously established literature values will be validated, and previously unavailable parameters will be calculated using first-principles energy approaches. In Year 1, such approaches will also be used to understand indium incorporation on non-polar vs. polar GaN planes, which has been experimentally observed to vary widely.

Progress Toward Milestone:

The modelling efforts led by Prof. Van de Walle at UCSB primarily focused on the problem of potential non-radiative Auger recombination in LED structures, which has been posited to contribute to LED efficiency 'droop' at elevated current density. Unlike previous modelling efforts, UCSB's approach was truly a first-principles *ab initio* methodology, in effort to eliminate uncertainty from modelling predictions. Building on solid numerical foundations, the Auger recombination rates of $In_xGa_{1-x}N$ were calculated from first-principles density-functional and many-body-perturbation theory. The differing mechanisms of inter- and intra-band recombination were found to affect different parts of the emission spectrum. In the blue to green spectral region and at room temperature the Auger coefficient can be as large as 2×10^{-30} cm^6 s^{-1}; in the infrared it is even larger. These results indicated that Auger recombination may be responsible for the loss of quantum efficiency that affects InGaN-based light emitters, whether non-polar or polar.

PROJECT ACTIVITIES

Inlustra Technologies

Due to delays in paperwork processing at DoE, the cooperative agreement was not received by Inlustra until 11/13/07; the agreement was accepted and signed by Inlustra on 11/14/07.

Initial growth development focused on heteroepitaxial a-plane and m-plane GaN thick films. Such films would later act as template layers for subsequent defect reduction by lateral epitaxial overgrowth (LEO). An emphasis was first placed on obtaining smooth film surface morphology, independent of underlying microscopic defect density (in the form of threading dislocations and stacking faults) and film growth rate. Variation of key hydride vapor phase epitaxy (HVPE) growth parameters such as temperature and V/III ratio (molar ratio between N and Ga precursors, respectively) led to the growth of smooth and transparent a-plane GaN thin films, such as shown in Fig. 1. Despite achieving such specular growth for a-plane GaN, additional refinement of process parameters was anticipated to yield higher quality films.

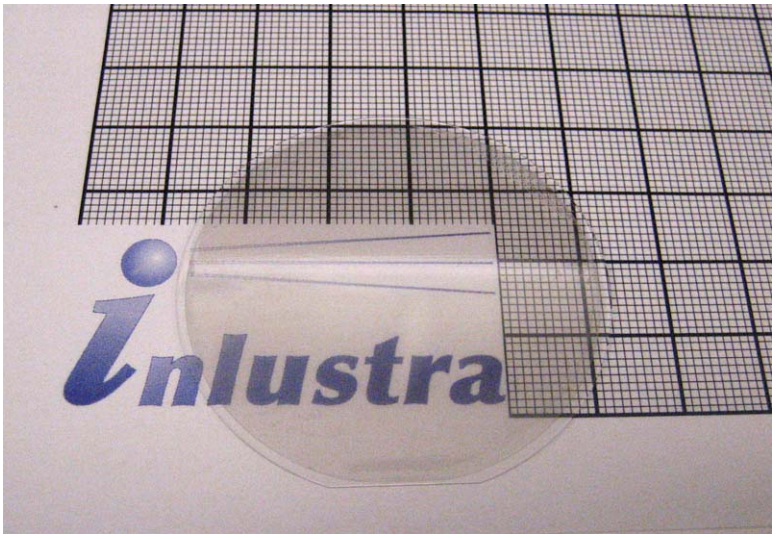

Fig. 1. Digital photograph of an a-plane GaN film grown on a 2-inch r-plane sapphire substrate.

Figure 2 below shows a Nomarski optical contrast micrograph of one of the *a*-plane GaN films. In some films such as this, sub-surface cracks were visible, which healed later in the growth. This acted as a stress-relief mechanism, and was consistent with observations originally made by Senior Investigator Haskell *et al.* at UCSB.

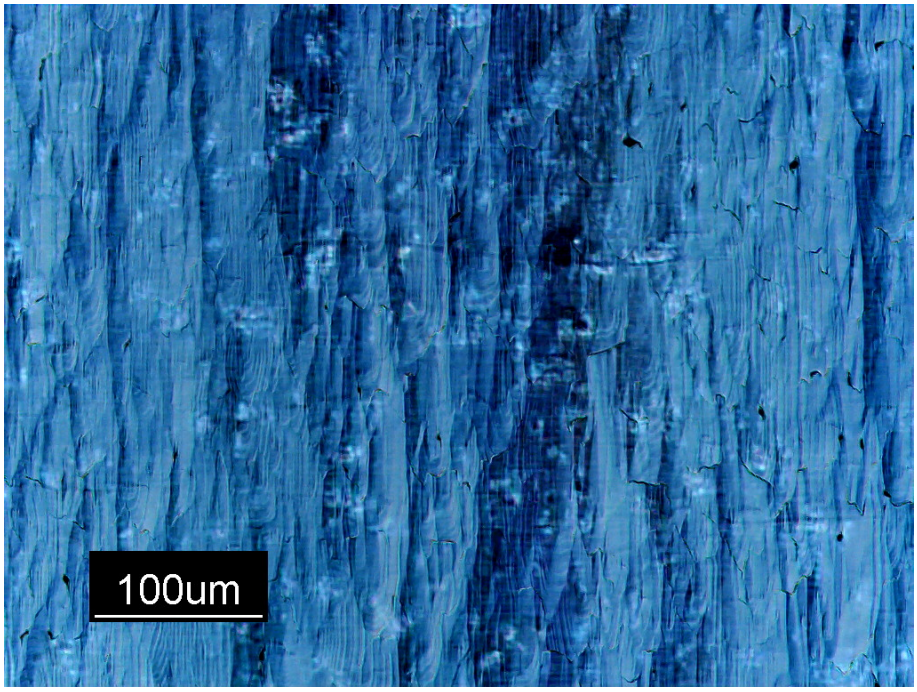

Fig. 2. Nomarski contrast optical microscope image of an HVPE a-plane film. Note that some sub-surface cracks are visible, which subsequently 'healed' during the growth process.

Early materials characterization was primarily concerned with surface morphology, both at the macro- and micro-scale. Figure 3 is an atomic force micrograph of the film shown in Fig. 2, and demonstrates the low root-mean-square surface roughness that can be achieved through HVPE growth parameter optimization. In this case, particular attention was paid to the ratio of ammonia (NH_3) and gallium chloride ($GaCl_x$) flows in the HVPE chamber.

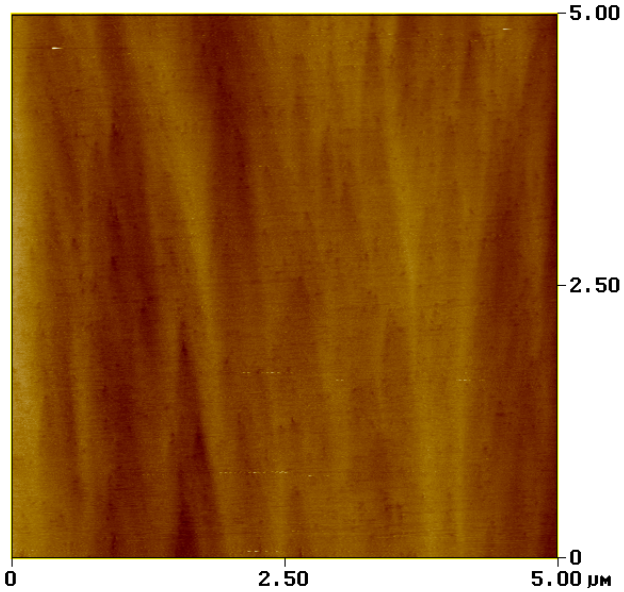

Fig. 3. Atomic force micrograph of an a-plane GaN film with 5 x 5 µm lateral extent and a z-range of 14.6 nm. The RMS roughness was 1.14 nm.

HVPE studies at Inlustra continued to primarily focus on uniform growth of smooth *a*-plane GaN films on 2-inch r-plane sapphire substrates. The emphasis shifted to increasing layer thickness while not sacrificing surface roughness to a great extent. To that end, Nomarski optical contrast microscopy was utilized for initial analysis, while AFM was applied to smoother samples, as described earlier. In addition, structural characterization expanded to the use of x-ray diffraction (XRD), which provides rapid, large-area feedback on microstructural quality. The primary type of XRD scan that was used was rocking curves, which quantify the degree of mosaic spread (disorder in the single crystal) due to microscopic defects such as threading dislocations. In Fig. 4, the on-axis rocking curve of a 50 μm thick a-plane GaN film is shown, which had a full width at half maximum (FWHM) of 0.12°. This value compares quite favorably with typical rocking curves measured in previous a-plane GaN growth research at UCSB. In addition, the off-axis 112 scan, which is influenced more heavily by the presence of pure-edge threading dislocations, had a FWHM of 0.37°. This value is quite acceptable for an a-plane GaN film of this thickness.

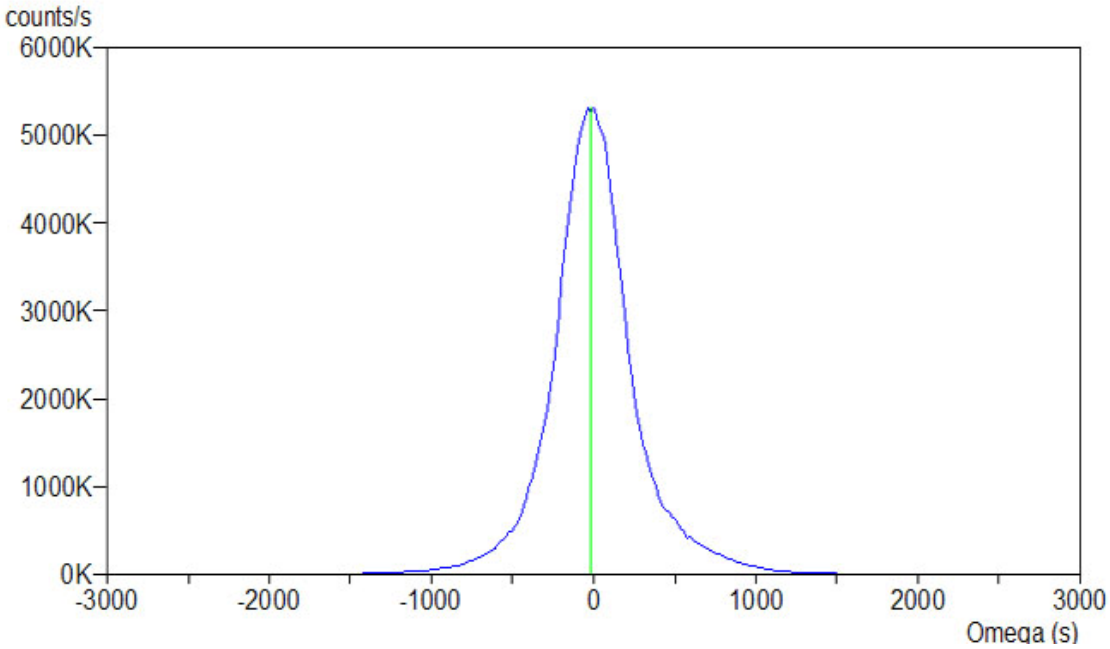

Fig. 4. X-ray diffraction rocking curve of the 110 (a-plane) peak, which exhibited a full width at half maximum of 0.12°.

While HVPE GaN growth studies at Inlustra continued to primarily focus on uniform growth of smooth *a*-plane GaN films on 2-inch r-plane sapphire substrates, lateral epitaxial overgrowth (LEO) growth runs were also started. A-plane GaN films with sufficiently smooth surfaces were coated with SiO_2, which was then periodically patterned and etched with open stripes of varying width and repeat period. Based on prior studies by co-investigator Haskell while at UCSB, the stripe orientation was chosen as <1$\underline{1}$00>, or the m-direction. Re-growth was performed on these patterned masked films under the same conditions used for planar a-plane films, with a typical

result shown in Fig. 5 below. In this sample, coalescence of neighboring stripes was almost complete, with semi-polar facets remaining in some elongated pits/trenches. The degree to which such pitting occurred varied over the film surface.

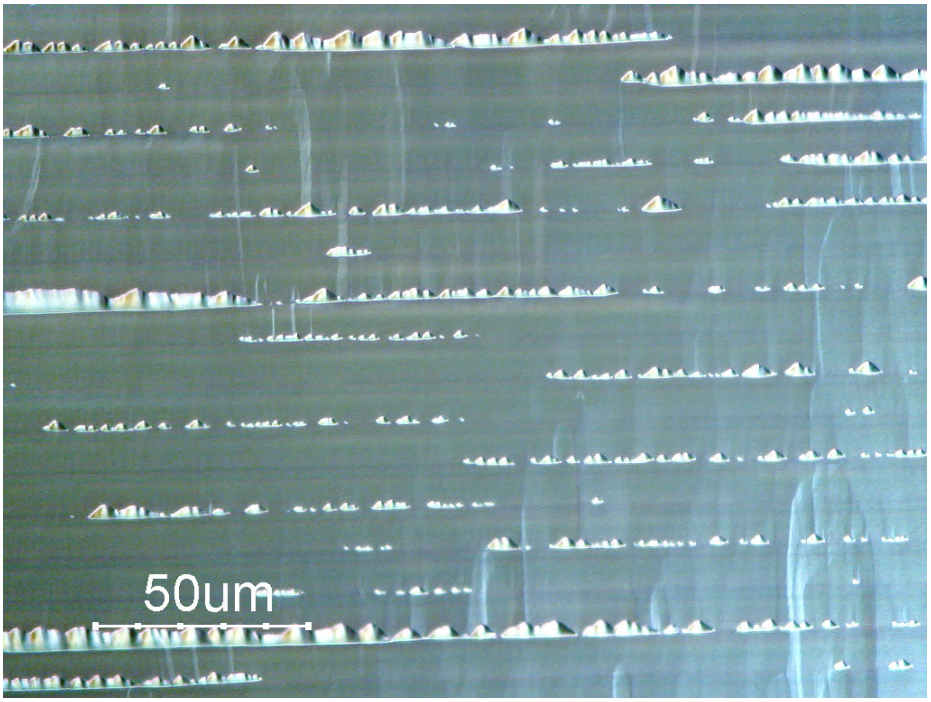

Fig. 5. Nomarski optical micrograph of a nearly coalesced *a*-plane LEO sample.

Additional LEO re-growth studies were conducted on SiO_2-masked samples with stripes patterned in the <1$\underline{1}$00> direction, with 2 µm openings and 8 µm repeat period. While we primarily focused on the smoothness of coalescence between neighboring re-grown GaN stripes, we also began microstructural characterization of coalesced LEO films. XRD rocking curves were measured in an orientation perpendicular to the stripe direction. As studied extensively by senior investigators Fini and Haskell while at UCSB, the presence of 'wing tilt', or crystallographic misorientation of over-grown areas relative to the underlying GaN film, can be readily measured with XRD. Any misorientation beyond the background mosaic (disorder) of the starting GaN film is undesirable, since microstructural defects such as dislocations will be formed at stripe-stripe coalescence boundaries. As shown in Fig. 6 below, we did not observe wing tilt for typical coalesced LEO films, which is a promising indication for further processing and/or re-growth.

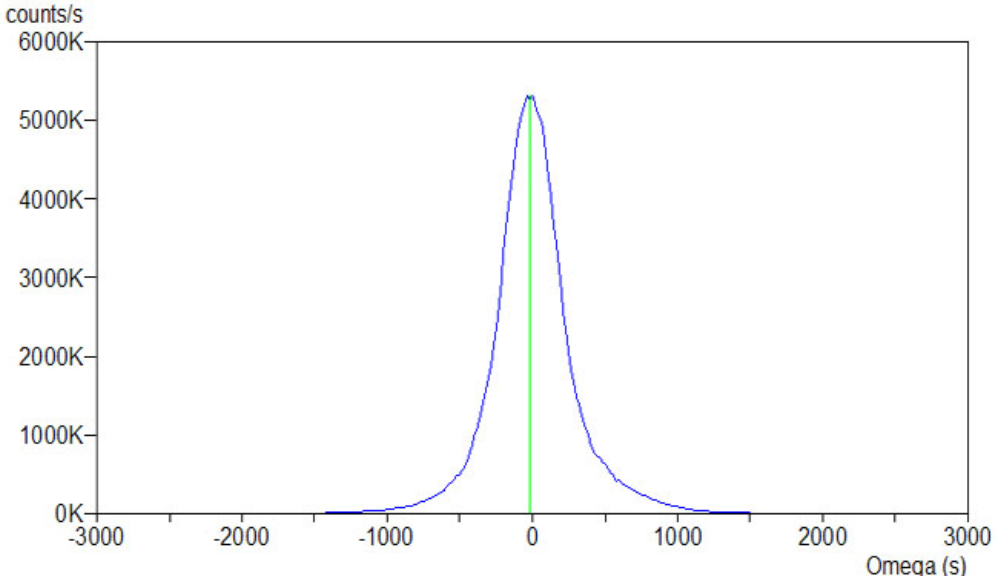

Fig. 6. XRD rocking curve of a coalesced *a*-plane LEO film, oriented in a direction such that the scattering plane is perpendicular to the LEO stripe direction. The full width at half maximum for this single peak is 0.187°.

In the third month of the second quarter, extended crystal growth system downtime due to a failed furnace element caused unexpected delays in experimental progress. Subsequently, while a-plane GaN LEO studies were continued, Inlustra personnel also began planar *m*-plane GaN film growth optimization. Initial growth studies resulted in fairly rough films (see *e.g.* Fig. 7), but HVPE growth parameter optimization was begun to improve surface smoothness for subsequent LEO processing and regrowth. Based on our team's previous *m*-plane GaN growth experience, primary attention was paid to the effects of growth temperature and V/III ratio, *i.e.* the molar ratio of N-containing to Ga-containing precursors. The ongoing goal was to maintain reasonably smooth surface morphology at growth rates exceeding 50 μm/hr.

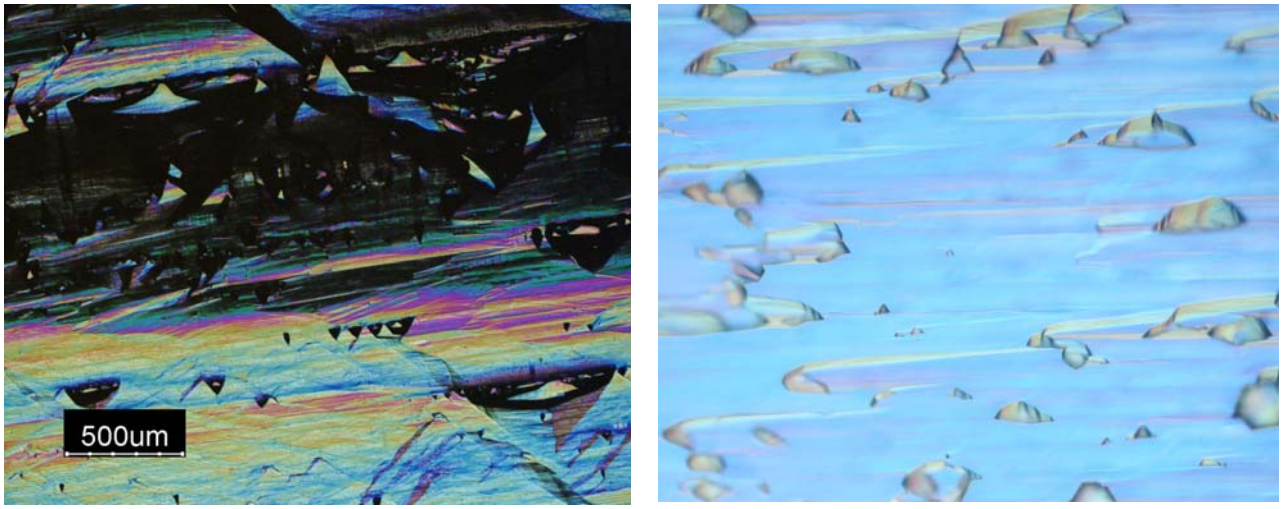

Fig. 7. Nomarski optical micrographs of rough *m*-plane GaN films, in which pits and surface ridges are visible. While such surfaces require improvement, these thick films are nearly fully coalesced and can be used for polishing studies (see below).

While obtaining smooth GaN surface morphology was a recurring priority in growth studies, rougher films are still of use for lapping and polishing research, whether for LEO patterning or planar film re-growth. We thus began initial polishing studies using conventional media such as SiC, diamond, and Al_2O_3 to determine the degree of polishing needed for HVPE re-growth of smooth, damage-free GaN. Later, we attempted quantifying key surface characteristics (*e.g.* residual RMS roughness) that needed to be measured for successful re-growth.

Inlustra continued its *m*-plane GaN film growth optimization, with an emphasis on obtaining smooth surface morphology at appreciable growth rates. HVPE growth conditions (particularly temperature and NH_3 flow) were systematically altered to understand the primary factors for obtaining reproducibly smooth *m*-plane surfaces. Smoother thick films (*e.g.* Fig. 8) were obtained, but further development was needed for direct use in LEO studies. In addition, some rougher films were used for lapping/polishing work (see below).

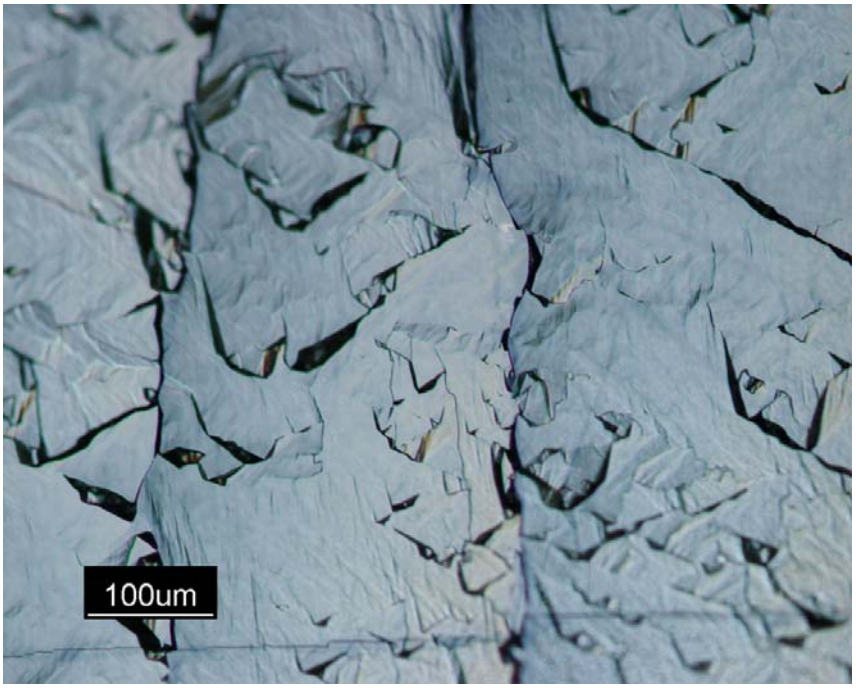

Fig. 8. Nomarski optical micrograph of a recent *m*-plane GaN film, in which surface features such as faceted pits are visible.

As mentioned above, growth of smooth non-polar GaN films remained a recurring priority in Inlustra's research. However, rougher (*e.g.* RMS > 50 nm) films were found to still be of utility for LEO patterning by first lapping and polishing them to sufficiently low residual roughness. Our recent in-house polishing studies used conventional SiC, diamond, and Al_2O_3 media of progressively smaller size, and yielded promising initial results. While optimization was still needed to remove distributed sub-micron sized surface pits, areas between pits are quite smooth, as shown in Fig. 9 below. We anticipated that further polishing work would result in surfaces uniformly smooth enough for film re-growth, wherein planarity will be maintained.

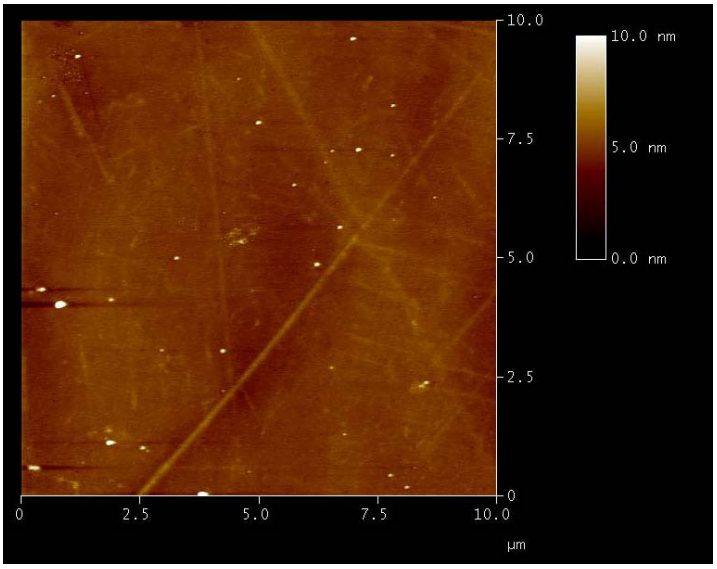

Fig. 9. AFM scan of an initially rough *a*-plane GaN film which was smoothened with conventional polishing media of progressively smaller size. Z-scale of 10 nm is indicated on the right.

Inlustra's non-polar GaN HVPE growth effort transitioned to producing free-standing *a*-plane thick films. We observed that in cases where widespread cracking in the *a*-plane GaN and/or r-plane sapphire did not occur, residual bowing for thicker (>100 µm) *a*-plane GaN films could hinder the uniformity of subsequent photolithographic processing. Likewise, if such samples were to be polished, a sufficiently small radius of curvature could cause non-uniform surface miscut and thickness variation to be induced, as depicted in Fig. 10. Therefore, we pursued the growth of very thick (> 500 µm) *a*-plane GaN films, followed by mechanical separation from the *r*-plane Al_2O_3 substrate.

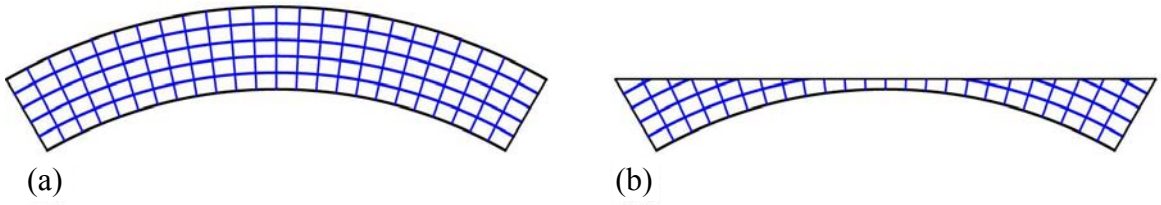

Fig. 10. Exaggerated schematic of (a) heavily bowed free-standing GaN wafer, and (b) non-uniform thickness and surface miscut induced by lapping/polishing such a wafer. Blue lines depict crystal lattice planes.

Wafer bowing before and after removal of the *r*-plane sapphire substrate was readily quantified by a few methods, including stylus profilometry (available in the UCSB cleanroom) and x-ray diffraction (also at UCSB). We pursued the latter approach, since it is non-contact and could be performed at the same time as other necessary XRD measurements. A 'knife edge' was first moved very close to the sample in order to verify that a small area was being sampled by x-rays. The position of the on-axis diffraction peak (in this case the 11$\underline{2}$0) was recorded, and the sample was then translated so a different position was measured. Sample bowing caused tilt of the local crystal lattice planes to differ from the first set of planes, and therefore the peak position

varied systematically over the sample. The angular difference between the peak positions was directly correlated with the radius of curvature of bowing. Since the in-plane mechanical properties of the *a*-plane GaN film differed depending on direction, this bowing measurement was recorded in two orthogonal orientations – one in the *c*-axis azimuth, and one in the *m*-axis azimuth.

While Inlustra continued its efforts at obtaining thick, free-standing *a*-plane films, we also furthered LEO studies for extended defect reduction. Specifically, we focused on "Sidewall" lateral epitaxial overgrowth (S-LEO) of *a*-plane films, which offers the potential of uniform microstructural defect reduction in a single re-growth step. As depicted in Fig. 11 below, a 100 nm thick SiO_2 mask was deposited on smooth *a*-plane GaN films, and then patterned into periodically repeated stripes of various widths and repeat periods (*e.g.* 5 µm opening, 35 µm repeat). The samples were etched in a Cl_2 plasma (reactive ion etching chamber) to define periodic trenches in the GaN film. Re-growth in the HVPE chamber was then conducted, which nominally began from the Ga- and N- polar c-plane sidewalls of the trenches.

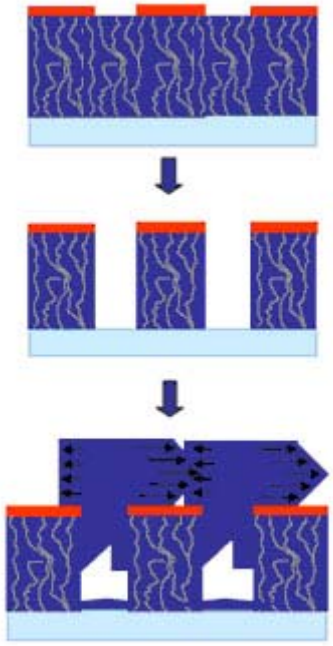

Fig. 11. Schematic of the S-LEO technique, in which a planar *a*-plane GaN film is masked, patterned, and then selectively etched. Re-growth occurs from c-plane sidewalls and emerges over the mask, such that low dislocation density results in large areas.

As shown in Fig. 12 below, initial re-growth results were promising, though coalescence of neighboring stripes was not entirely uniform. The manner of initial re-growth from sidewalls needed further study, since an undesirable morphology that initially evolves may be difficult to remove with subsequent growth. Later, structural characterization such as atomic force microscopy (AFM) and transmission electron microscopy (TEM) was performed to quantify the extent and uniformity of dislocation reduction.

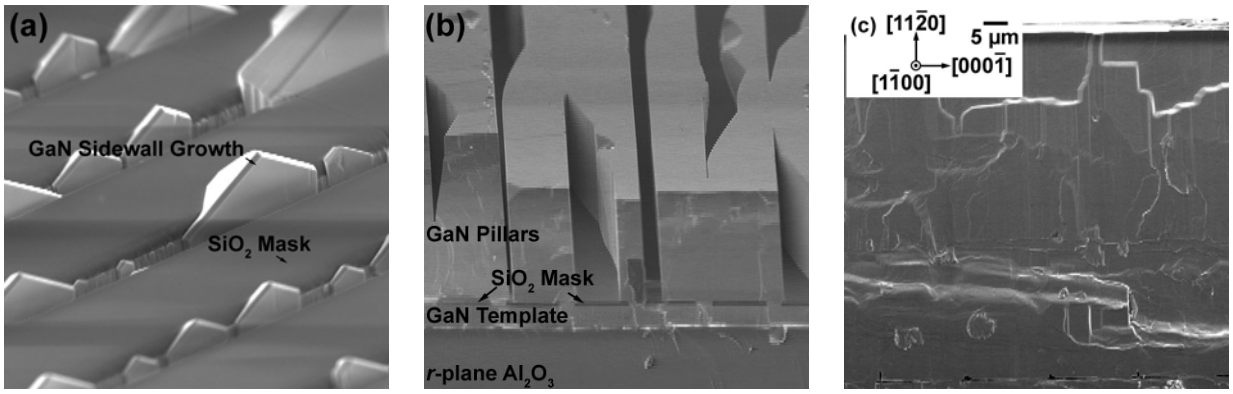

Fig. 12. Scanning electron microscope (SEM) images of S-LEO films. (a) sidewall nucleation stage; (b) planar pillar lateral growth and beginning of coalescence; and (c) cross-section of coalesced S-LEO film (surface features are cleaving artifacts).

While still in the process of optimizing S-LEO coalescence uniformity and smoothness, Inlustra also polished some un-optimized coalesced samples to evaluate their potential for device re-growth. Polishing with conventional media yielded surfaces that were promising, as shown in the AFM micrograph in Fig. 13 below. A few scratches remained, but average roughness (~ 0.2 nm RMS) was low overall. Further refinement was expected to lead to planar, smooth surfaces suitable for LED layer re-growth by MOCVD.

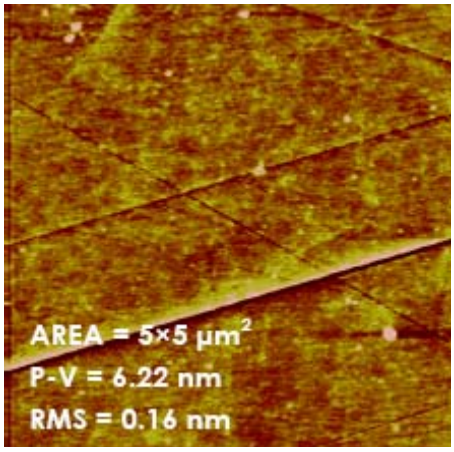

Fig. 13. Atomic force micrograph of a 5x5 µm area of a polished S-LEO sample, in which a few scratches remain but RMS roughness is low.

While pit-free, "seamless" stripe-stripe coalescence was not yet fully achieved, focus shifted to the effectiveness of dislocation and stacking fault reduction in these films. Although transmission electron microscopy (TEM) was to be utilized on the 'best' films, it is an expensive, slow technique, requiring special sample preparation and microscopic analysis. As a screening technique with rapid turnaround, we utilized cathodoluminescence (CL), a method in which light is emitted from a sample excited by the electron beam in a scanning electron microscope. Via this light emission, low-defect areas are visibly bright, whereas dislocations and stacking faults are visible as dark lines or spots. Spatial resolution of a few hundred nanometers is possible, and is limited by the minority carrier diffusion length. As show in Fig. 14 below, CL can provide valuable preliminary information on the effectiveness of defect reduction in GaN LEO films.

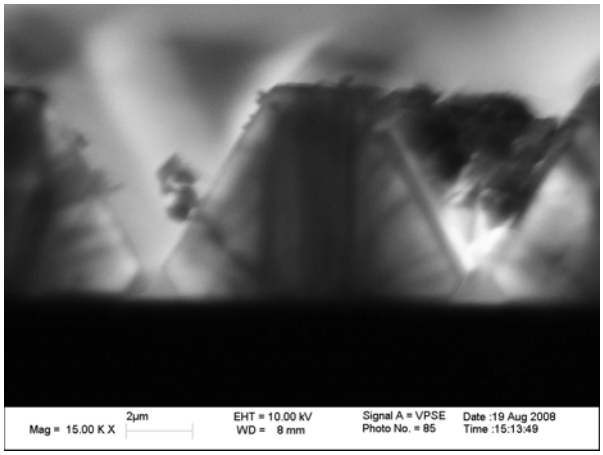

Fig. 14. CL image of a cleaved LEO cross-section, in which dislocations are visible as dark lines, and brighter areas are nearly dislocation free. Visible debris is particulate generated by the cleaving process.

Efforts at Inlustra focused on quantifying the effectiveness of the currently developed *a*-plane and *m*-plane LEO techniques in lowering dislocation density to the target level of 5 x 10^6 cm^{-2}. To this end, AFM and CL were performed as 'screening' techniques. As detailed above, via CL dislocations are often visible as dark lines or points relative to the surrounding lighter areas with few defects. TEM, which is a more quantitative but also more time-consuming and expensive technique, was then performed on promising samples. As shown in Fig. 15 below, we found that for single-step coalesced ***a*-plane** 'Sidewall' LEO (S-LEO), large overgrowth regions were nearly defect free, and numerous TEM measurements revealed an average dislocation density of **2-3 x 10^6 cm^{-2}**. We note that the average stacking fault density was measured as approximately **5 x 10^3 cm^{-1}**. However, at this time we were are not actively seeking to reduce this density, since we had not seen data in the literature to suggest that stacking faults are deleterious to LED performance.

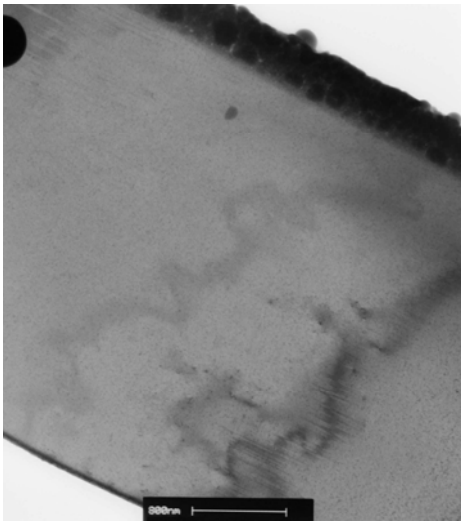

Fig. 15. Cross-sectional TEM micrograph of an overgrown region in an *a*-plane S-LEO sample, with a diffraction vector of g = 1$\underline{1}$00. Visible dark, wavy features are artifacts of bending contrast in the thin TEM foil.

TEM was also performed on *m*-plane LEO samples, an example of which is shown in Fig. 16. Here a clear threading dislocation reduction to **~4 x 10^6 cm^{-2}** was observed, thus demonstrating the effectiveness of our LEO development to date. Stacking faults, visible in Fig. 16 as vertical lines, were present at a density of **~ 5 x 10^5 cm^{-1}**, which was higher than that observed in *a*-plane S-LEO samples. However, as noted above, this was not of concern until evidence clearly showed that LED performance suffers from the presence of stacking faults.

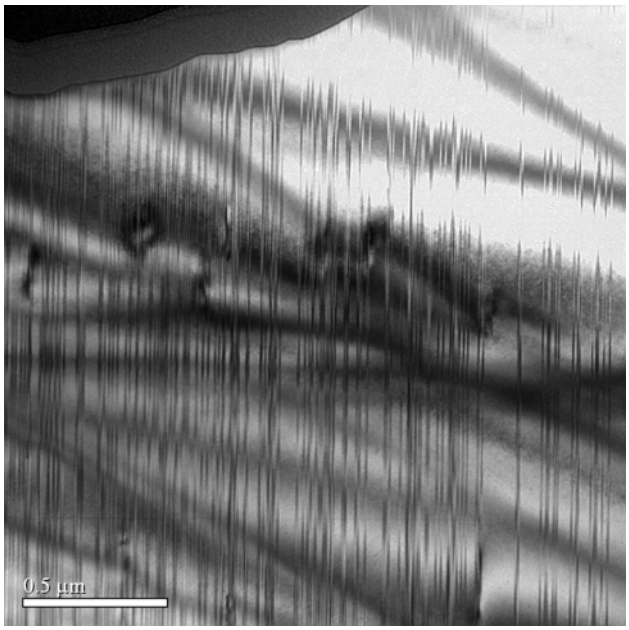

Fig. 16. Cross-sectional TEM micrograph of an overgrown region in an *m*-plane GaN LEO sample, with diffraction vector g = 0002. Vertical lines are stacking faults, and dark oblique features are due to bending contrast in the thin TEM foil.

Although Inlustra met its dislocation reduction milestone via lateral epitaxial overgrowth (LEO) processing and re-growth, at our own expense we also investigated the technique of cross-cutting as a means of wide-area dislocation reduction. This approach relied on the growth of a sufficiently thick (e.g. > 5mm) but defective GaN crystal, followed by cutting and polishing in an orientation perpendicular to the original growth surface. The resulting wafers, in this case *m*-plane GaN slices cut from a thick *a*-plane crystal, now had all previous dislocations lying within the plane of the wafer, and thus they did not propagate into the overlying re-grown device layers. However, stacking faults, whose effect on the electrical and optical behavior of LEDs and laser diodes is not yet known, propagated into the re-grown film.

UCSB – LED growth, fabrication

The LED growth and fabrication effort at UCSB was delayed multiple times due to facilities outages related to an ongoing construction project adjacent to the MOCVD laboratory. Between planned (and unplanned) facilities shutdowns as well as building-wide electrical outages related to the Gap wildfire, insufficient growth time was able to be allocated to this part of the project. Nevertheless, as described below significant progress was made in optimizing growth conditions of blue and blue-green LEDs on m-plane wafers provided by Inlustra.

Early in the UCSB growth effort, *m*-plane GaN films were grown on ZnO buffer layers deposited on *m*-plane Al_2O_3 substrates by metalorganic chemical vapor deposition (MOCVD). Diethylzinc (DEZ) was used as the zinc precursor and pure O_2 was used as the oxygen precursor. Nitrogen was the carrier gas. The ZnO buffer layer was grown at 400°C at a reactor pressure of 50 Torr. Once the ZnO buffer layer thickness reached 300nm the temperature and pressure were increased to 650°C and 760 Torr, respectively, for the deposition of a 1 μm thick low-temperature GaN layer. Trimethylgallium (TMG) and high purity ammonia (NH_3) were used as the Ga and the N precursor, respectively. The purpose of this low-temperature GaN layer was to protect the underlying ZnO surface buffer from decomposing once the growth temperature was increased to the nominal GaN growth temperature (1050°C in these experiments). The pressure was decreased to 50 Torr before the growth of the actual GaN layer started. This layer was 2-2.5 μm thick.

Figure 17 shows an atomic force microscopy (AFM) micrograph of a 20×20 μm^2 area of the surface of an m-plane GaN/ZnO sample. The surface exhibited large micrometer-sized islands, indicating a three dimensional (3D) growth mode.

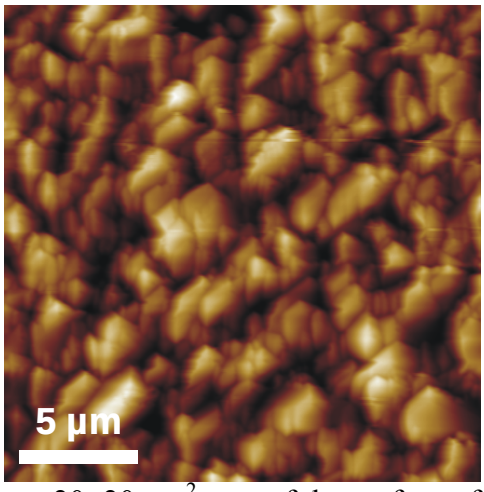

Fig. 17. AFM micrograph over a 20×20 μm^2 area of the surface of an *m*-plane GaN sample. The surface exhibits large micrometer-sized islands indicating a three dimensional (3D) growth mode. The surface of each individual island is smooth.

Figure 18 shows an XRD ω-2Θ scan for the 1$\underline{1}$00 reflection. A clear but broad *m*-plane GaN peak was observed. The full width at half maximum (FWHM) was 0.45° (1620 arcsec). The small peak to the right of the main peak indicates that the layer was not entirely phase pure; at least one other GaN orientation (likely c-plane) was present.

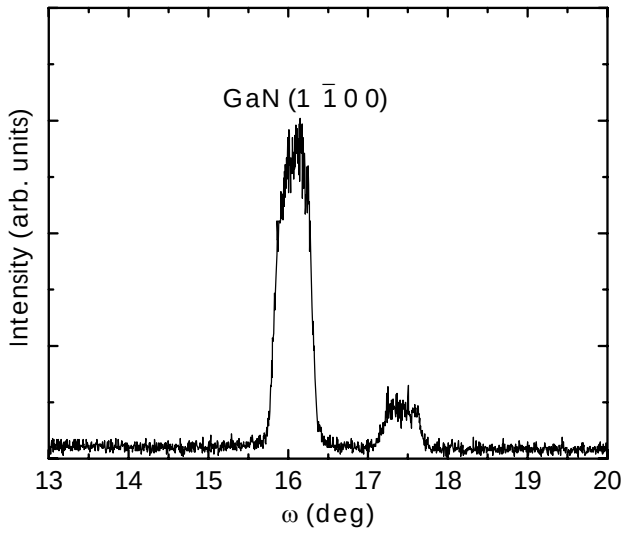

Fig. 18. XRD ω-2Θ scan for the 1$\underline{1}$00 reflection of an *m*-plane GaN/*m*-plane ZnO film. A clear but broad m-GaN peak was observed.

MOCVD growth of non-polar m-plane GaN films on m-plane GaN wafers provided by Inlustra was soon initiated. These MOCVD films were 2 μm thick and were grown at a susceptor temperature of 1165°C and a reactor pressure 760 Torr. The flows of ammonia and Ga (TMG) were 6 splm and 40.5 sccm, respectively. No low-temperature nucleation layer was used. These growth conditions correspond to standard **c-plane** GaN growth conditions. Figure 19 shows an AFM micrograph of a 20x20 μm area of the surface of an m-plane GaN film. The surface exhibited ridges which were 240-340 nm high (peak-to-valley) and 2.4-3.6 μm wide. This surface morphology needed improvement, but was considered promising for initial attempts at homoepitaxial base layers for LED re-growth.

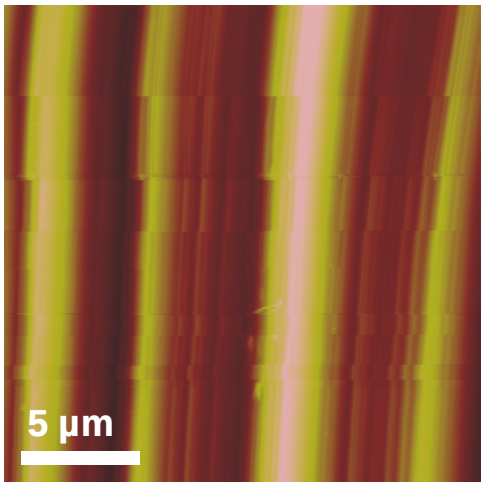

Fig. 19. AFM micrograph of a 20x20 μm area of the surface of a re-grown homoepitaxial m-plane GaN film.

Next, MOCVD reactor-specific growth effects were investigated by re-growing m-plane GaN films on m-plane GaN wafer supplied by Inlustra in a different reactor type. The growth conditions were generally comparable to those above (760 Torr reactor pressure, same precursor flows, no nucleation layer). Figure 20 shows an interference contrast optical micrograph (~200x magnification) of the resulting surface. The striated surface morphology was essentially identical to the initial growth experiments. This indicated that at this stage, the reactor type had less impact on the surface morphology as compared to the growth conditions.

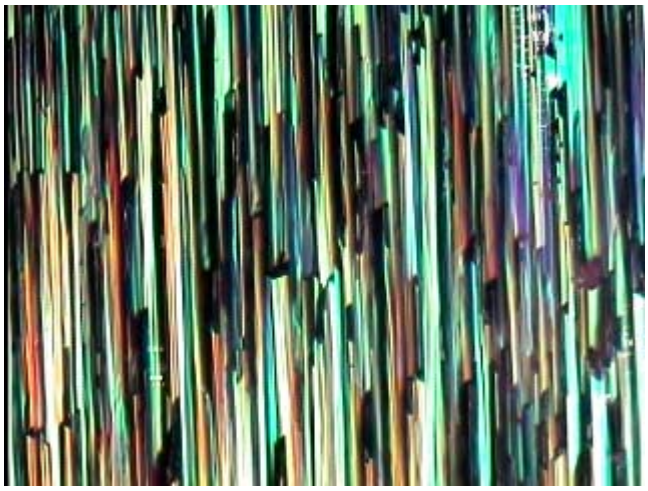

Fig 20. Interference contrast optical micrograph (200× magnification) of the surface of an m-plane GaN films grown in a different type of MOCVD reactor.

Intermittent MOCVD system downtime continued to be a problem, but within a few weeks t laboratory facilities work was completed and LED growth studies could be continued. While waiting for this to occur, a full m-plane LED structure was grown on a 'borrowed' MOCVD system in a neighboring laboratory, using growth conditions adapted for that particular reactor. The LED was grown on an m-plane GaN wafer provided by Inlustra which had an average threading dislocation density estimated at lower than ~1 x 10^6 cm^{-2}. The device active region consisted of 8 nm thick GaN barriers and 5 nm thick $In_{0.17}Ga_{0.83}N$ wells.

Figure 21 shows a photoluminescence (PL) spectrum of the grown LED structure. The peak emission wavelength was centered at 484 nm, which was fairly close to the expected peak wavelength (~470-475 nm) for this device structure. The peak's full width at half maximum was 37 nm, which is comparable to previously grown structures. These PL characteristics were promising, and indicated that full LED fabrication and electroluminescence testing should proceed.

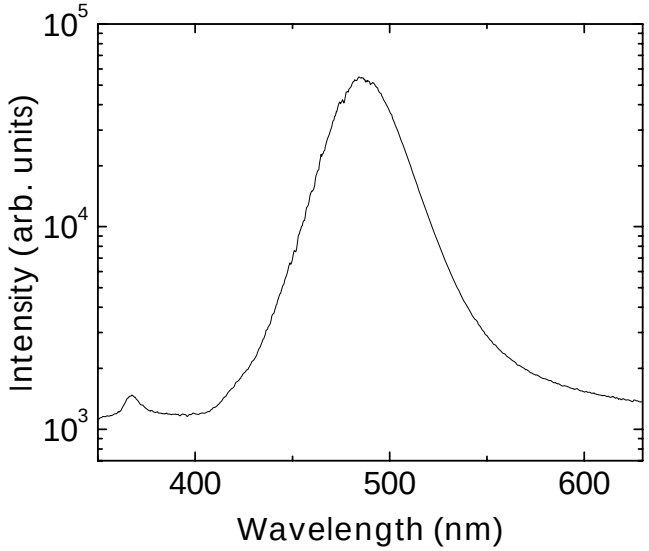

Fig. 21. PL spectrum from an LED structure grown on an Inlustra *m*-plane wafer; **note that intensity axis has a log scale**. The peak emission wavelength was centered at 484 nm and the peak FWHM was 37 nm.

This LED structure was processed in the cleanroom in order to improve the contact properties relative to the 'quick test' In dot approach. Metal Pd/Au contacts were deposited on the p-type side of the LED. Mesas were defined and etched down to the underlying n-GaN layer. However, results from the subsequent I-V probe (electroluminescence) measurements showed that the structure was electrically shorted. Most likely this was due to the very rough surface morphology which shorted the p- and n-regions of the LED. Near-term growth plans were made to focus on improving this morphology by altering MOCVD growth conditions.

Williamson-Hall XRD analysis was employed to assess the density of basal plane stacking faults (BPSF) in *m*-plane wafers supplied by Inlustra. X-ray rocking curve FWHM values were recorded for the on-axis reflections $10\underline{1}0$, $20\underline{2}0$ and the $30\underline{3}0$. The XRD scans were performed with the beam direction parallel to the a-axis ($\Phi=0°$) and the c-axis ($\Phi=90°$). The latter measurement is sensitive to the lateral coherence length which in turn depends on the basal plane stacking fault density. The FWHM values are plotted in Fig. 22. The intercept of a linear fit applied to each group of measurements represents the lateral coherence length. From this plot the lateral coherence length was determined as 29.6 nm, which corresponds to a stacking fault density of $\sim 3\times10^5$ cm^{-1}. This value is comparable to that obtained in TEM measurements described above.

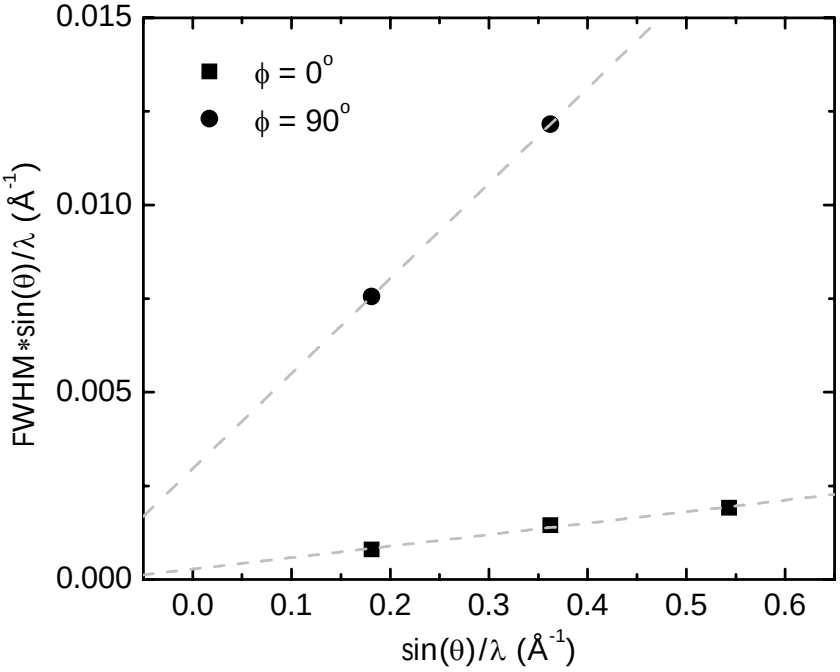

Fig. 22. XRD rocking curve FWHMs from Williamson-Hall measurements for a cross-cut m-plane GaN wafer.

Another light emitting diode (LED) structure was grown following an established LED recipe, with the goal of maximizing emission wavelength. Electrical testing showed a short circuit behavior between the p- and n-contacts of the LED. Hence, no electroluminescence was observed. However, photoluminescence measurements showed a peak at 450 nm with a peak width of 40 nm, indicating that the active region itself was of adequate quality. We attribute the electrical shorting to surface roughness induced by MOCVD growth conditions that were not yet optimized for samples containing stacking faults. These faults, since their in-plane displacement direction is normal to the sample surface, perhaps acted as 'nucleation' points for micro-faceting. Such faceting caused the observed roughness. Efforts were then focused on circumventing this roughening effect by varying key growth parameters such as pressure, V/III ratio and temperature. Concurrently, we pursued optimization of the InGaN quantum wells themselves under such conditions, since significant shifts from previously established MOCVD parameters were anticipated.

Low Pressure MOCVD

Until this point, all non-polar GaN-based LED growth runs performed at UCSB in support of this project were done in a MOCVD system with an ambient at or near atmospheric pressure. These device films were rough to the degree that electrical shorting was observed during testing. After a number of false starts due to continuing facilities-related outages, UCSB now began intense efforts to develop low-pressure (LP) MOCVD growth conditions to improve the surface morphology of these non-polar LED films.

A reactor pressure of 67 Torr was chosen for all growths. Before full LED structures were deposited, 'building blocks' such as n- and p-type doped layers and quantum wells (QWs) were first developed. Magnesium doping for p-type conduction was optimized by depositing a multi-layer "SIMS stack", for which Secondary-Ion Mass Spectroscopy (SIMS) measurements revealed the physical Mg concentration vs. useful hole concentration as a function of depth in the film (see example in Fig. 23). Using this method, a 'reference' level for Mg concentration was obtained (~ 2 x 10^{19} cm^{-3}). Higher Mg incorporation levels would require replacement of flow components in this MOCVD system.

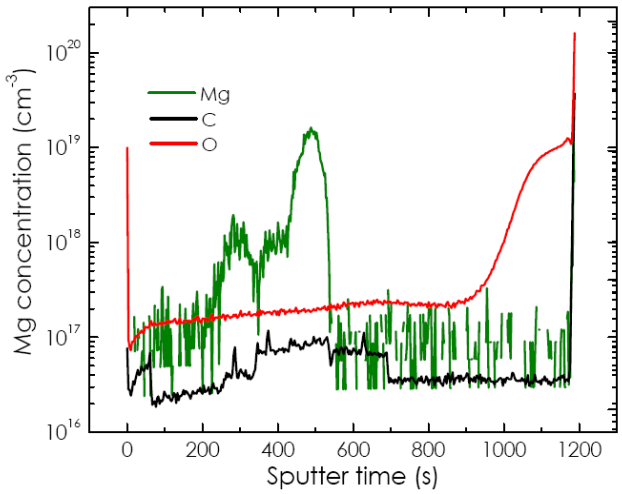

Fig. 23. SIMS depth profile for the species Mg, C, and O in an *m*-plane GaN film.

For InGaN QW development, a thick low-pressure grown buffer layer was first grown on Inlustra-provided *a*-plane and *m*-plane wafers before the deposition of InGaN/GaN (5×) multiple quantum wells using the same LP conditions. The behavior of Indium (In) incorporation was studied by photoluminescence and X-ray diffraction. LED structures were also grown and characterized, as detailed below. Electroluminescence was obtained from these LED structures grown under low-pressure conditions.

Photoluminescence

Figure 25 shows the photoluminescence spectra of four InGaN/GaN multiple quantum well (MQW) samples grown at successively lower growth temperatures (855-805°C) in order to study the trend of In incorporation. The MQW structure (Fig. 24) was based on a reference c-plane InGaN MQW design consisting of five periods of 3 nm InGaN well/9 nm undoped GaN barrier which yielded photoluminescence emission at 425 nm for an In content of 10-12%. The MQW stack was grown on a 2 μm thick buffer layer and was capped by a 12 nm GaN cap layer. Both the buffer layer and the quantum well structure were undoped.

thickness (nm)	layer	description	Structure
12	GaN	cap layer	
5×(3+9)	InGaN/GaN	MQW	
2000	GaN	buffer layer	
	m-GaN	substrate	

Fig. 24. Schematic of MQW structure used in the present study.

In a manner analogous to c-plane InGaN QWs, lower growth temperatures resulted in a shift toward longer PL emission wavelength. The MQWs grown on *m*-plane wafers with low dislocation density yielded narrower peaks, reflecting their higher overall quality. It is however difficult to assess the impact on the width due to the higher In content, since both extended microstructural defects and point defects may contribute. The wavelengths varied between 492-510 nm and the peak widths between 38-55 nm.

Figure 26 shows the corresponding XRD 2θ-ω scans for two of the samples. Satellite peaks due to the presence of the quantum wells are clearly visible. The QW period was calculated as 12 nm, which is consistent with the intended well and barrier thicknesses of 3 and 9 nm, respectively. The In content was calculated as 20-25%.

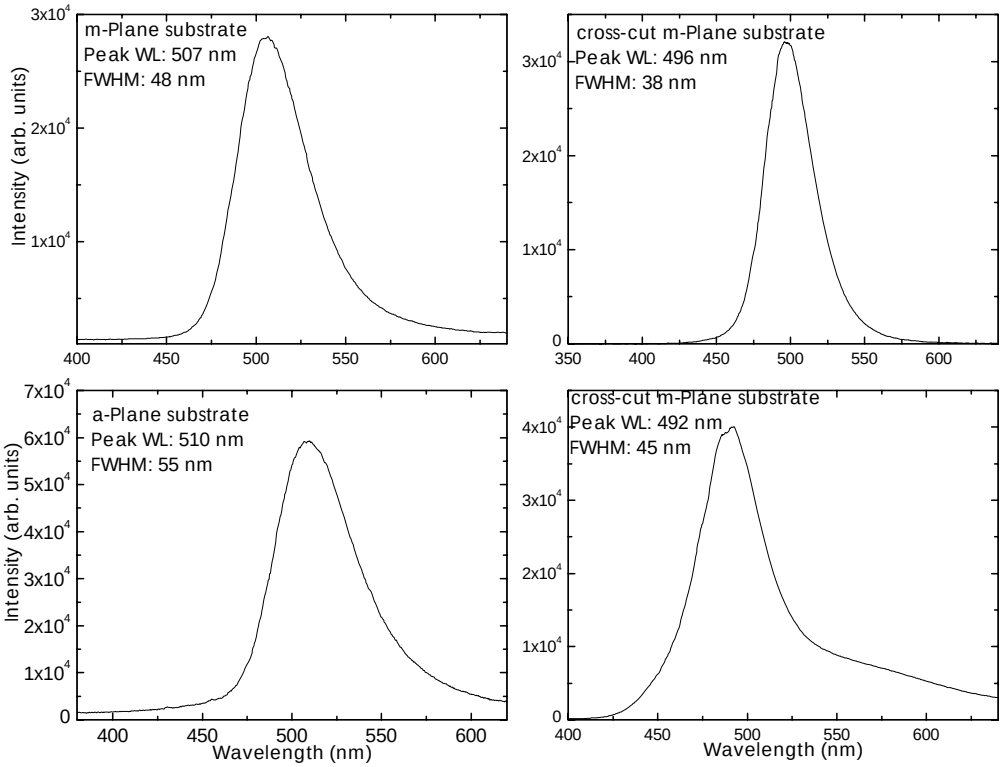

Fig. 25. Photoluminescence spectra from non-polar InGaN QWs grown at successively lower growth temperatures.

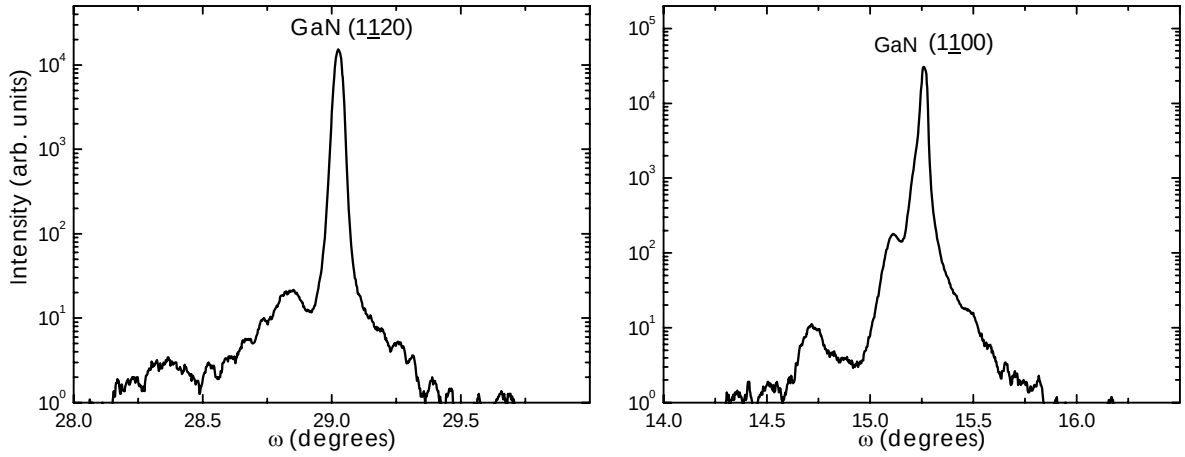

Fig. 26. XRD 2θ-ω scans of 5x InGaN/GaN quantum wells grown on a- and m-plane wafers.

Electroluminescence

Figure 27 shows the electroluminescence (EL) spectrum of a full *m*-plane InGaN/GaN LED grown at low pressure (67 Torr) on an m-plane substrate. The LED structure (Fig. 26) consisted of 3 periods of 3 nm InGaN well/12 nm undoped GaN barrier. Note that **initial EL testing was done with simple probe-on-wafer measurements**, *i.e.* no packaging was utilized for light extraction enhancement.

The forward voltage was 3.6V and 4.5V at a drive current of 5 and 20 mA, respectively. These values were reasonable at this early stage of development, and indicate that the p-type and n-type conductivity levels were adequate. The emission wavelength was 492 nm and the peak width was 36 nm. The power was measured on an unpackaged and unprocessed sample (*i.e.* no etched p-type mesa or vacuum-deposited contacts); soldered In dots were used as contacts. A raw power of 60 μW was measured with a Si photodetector.

thickness (nm)	layer	description	structure
20	GaN:Mg+	contact layer	
500	GaN:Mg	p-layer	
10	AlGaN	blocking layer	
3×(3+12)	InGaN/GaN	MQW	
2000	GaN:Si	n-layer	
5000	GaN	buffer layer	
	m-GaN	substrate	

Fig. 26. Schematic of InGaN/GaN LED structure used in present study.

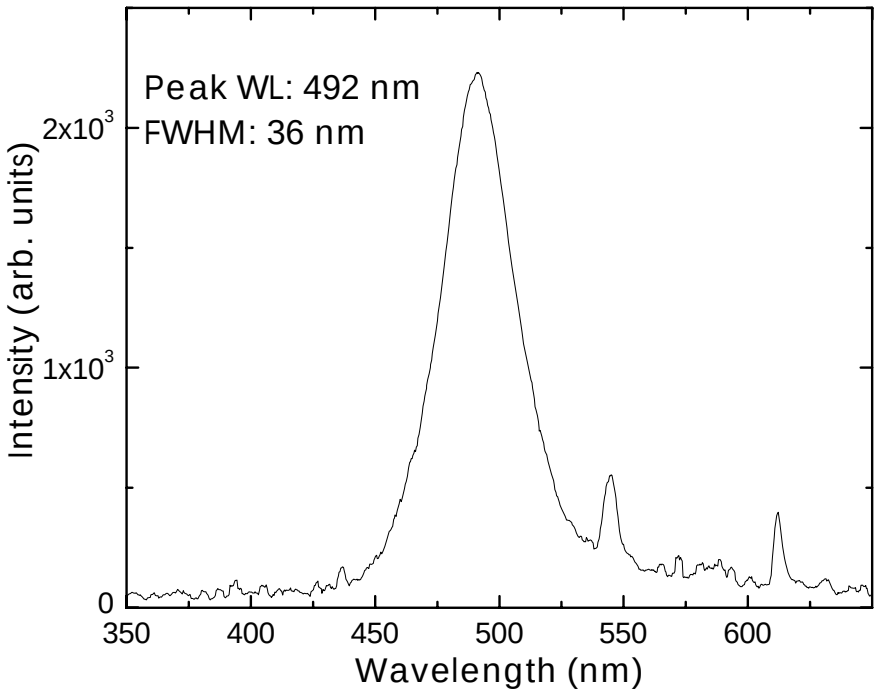

Fig. 27. Electroluminescence spectrum of a blue-green LED structure grown on an m-plane wafer.

Summary

Planar a- and m-plane heteroepitaxial films as well as reduced defect density m-plane GaN wafers were characterized structurally and morphologically. Buffer layers grown at low pressure by MOCVD on the substrates improved the surface morphology slightly relative to those grown at atmospheric pressure. MQWs grown at varying temperatures at low pressure on these buffer layers yielded a maximum PL emission wavelength of 507-510 nm, indicating that the In incorporation was not enough to reach longer wavelengths. In comparison, non-optimized c-plane MQWs grown under similar conditions exhibited PL emission wavelengths >515 nm.

All LED structures except one were electrically shorted but optically active as revealed by PL measurements. Electroluminescence of the working unpackaged LED was centered at ~492nm.

UCSB – Modelling

The subcontract paperwork between Inlustra and UCSB was finalized in December 2007, allowing the Sub-PI (Prof. Van de Walle) to move forward with final selection of research personnel. In the meantime, initial modelling activities were continued, with primary focus on key parameter identification and quantification. In addition, PI Fini and sub-PI Van de Walle discussed near- and long-term modelling topics specific to GaN device structures, vs. materials issues such as the influence of defects in these devices. The latter, being dependent largely on first-principles calculations, was agreed to be well suited to Prof. Van de Walle's established

expertise in the field. Therefore, the focus of non-radiative Auger recombination in GaN-based LEDs was decided on as the initial modelling topic in Year 1.

UCSB's modelling of Auger recombination loss in GaN-based light-emitting devices advanced significantly in the early months of 2008. The conflicting results of previously published studies as well as preliminary studies at UCSB showed that this issue is best understood via first-principles calculations such as Van de Walle *et al.* employ. Using many-body perturbation theory, they were able to compute accurate single-particle band structures for III-N semiconductors and, further, evaluate the Auger recombination rate. The band structure was computed using the GW approximation (see Fig. 28 below), which is the method of choice for obtaining accurate band structures in solids. Additionally, Auger transition matrix elements of the screened Coulomb interaction, *W*, were computed between four states. Electron-electron-hole Auger recombination, which was predicted to be the strongest process in nitride semiconductors, involves two free electrons in the conduction band, one of which recombines with a hole in the valence band – see Fig. 28. This results in an energy- and momentum-conserving transition of the second electron to a higher-lying conduction band. Preliminary results indicated that the theoretical Auger recombination rate is of the correct order of magnitude to explain the losses measured in published measurements.

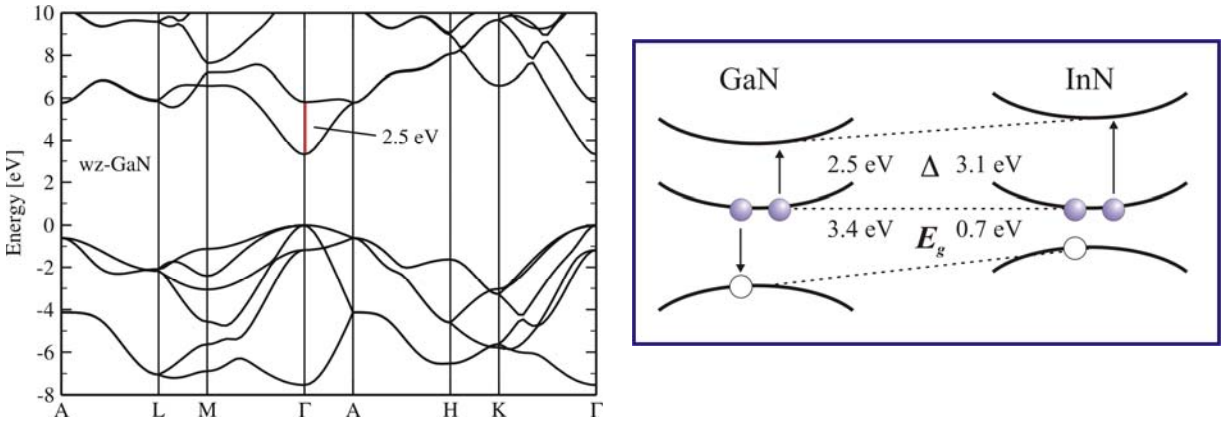

Fig. 28. Calculated GaN band structure via GW many-body perturbation theory (left) and a depiction of the posited non-radiative Auger transition (right). Blue circles represent electrons, and white circles are holes.

Subsequently, Van de Walle's team focused on improving the numerical efficiency of computing the high-dimensionality integrals involved in calculating the Auger recombination rate. The computation of the Auger rate required the evaluation of a 12-dimensional integral in momentum space. Momentum conservation reduced this to an integral in 9 dimensions, which was still formidably computationally expensive if carried out by standard quadrature methods. Moreover, the delta function resulting from the energy-conservation condition could not be directly evaluated numerically, and they found that replacing it with a narrow Gaussian introduced a bias in the result of the integral (and hence the Auger rate).

To overcome this computational bottleneck they implemented a Monte Carlo integration scheme. The delta function was evaluated analytically, which transformed the integration into an 8-dimensional surface integral in 9-dimensional space. The stochastic nature of the Monte Carlo scheme, where points in 8-dimensional space are generated randomly, reduced the computational

cost for high-dimensionality integrals, so that the error in the result was reduced as the square root of the number of samples (independent on the dimensionality of the space) and an estimate of the error was provided intrinsically by the method. Hence, the calculations were significantly more efficient and easier to converge than those involving direct quadrature. Van de Walle *et al.* then employed this new Monte Carlo method for computing the Auger rate of InGaN using an anisotropic effective-mass band model, with band parameters obtained from highly accurate many-body perturbation theory calculations.

UCSB performed final tests on its Monte Carlo integration scheme to evaluate the multidimensional integral required to calculate InGaN Auger recombination rates. At this stage of the simulations, they took the underlying band structure to be that of GaN, based on highly accurate many-body perturbation theory calculations. The effect of increasing indium concentration in the InGaN quantum well was modeled by reducing the band gap. The rate for inter-conduction-band processes was computed for electron and hole concentrations in the range of $1x10^{17}$-$1x10^{19}$ cm^{-3}; band occupations were calculated using Fermi statistics (unlike previous simulations of Auger rates that used Boltzmann statistics). In this range of carrier concentrations the Auger coefficient is roughly independent of the carrier density (see Fig. 3). This implies that even when Fermi statistics are used, the Auger rate remains proportional to the carrier density cubed. Thus for typical carrier densities in light-emitting devices, inter-conduction-band Auger recombination can be an important loss mechanism.

UCSB's Auger modelling effort later progressed to the point where the derivation of an analytic expression for the Auger recombination rate was finalized to cross-check the previous numerical implementation. For this approach, energy bands were assumed to be parabolic and isotropic and were populated according to Boltzmann statistics. In addition, the Auger transition matrix element, a key component of the rate calculation that details the interaction between the electrons and holes during the scattering event, was assumed to be independent of the particles' momenta. These simplifications were sufficient to analytically solve the Auger rate equation. After some rather tricky integrations, the result was a relatively simple expression, which only required electron and hole effective masses, as well as band gaps, as input parameters. The analytic model could then be used to efficiently scan the dependence of the Auger recombination rate on these parameters. Imposing the same restrictions in the full numerical code reproduced the analytic results, thus providing an important cross-check for the correctness of the numerical implementation (based on multidimensional Monte Carlo integrations, as described above). The analytical implementation also proved useful for scanning across a range of parameters and identifying physical trends.

The UCSB modelling team started investigating the role of alloying on InGaN Auger non-radiative recombination. Their initial attempts at understanding alloying were restricted to a simple linear variation in the band gap as a function of alloy composition. For initial studies, issues such as non-linear band-gap behavior (described by the bowing parameter), differences in carrier effective masses, and variation of the second conduction band were ignored. Their first efforts to improve the description of the role of alloying involved performing very accurate calculations of the band structure of 25%, 50% and 75% In alloys using a periodically repeated "supercell". The alloys that were input into calculations were ordered, but this enabled the collection of a number of data points for understanding band gap bowing. They also aimed to understand how this bowing should be applied to the second conduction energy band, which is entirely unknown from experimental spectroscopy.

In addition to features of the band structure, UCSB started to investigate how symmetry breaking due to alloying affects the Auger transition matrix elements. Interestingly, calculations showed that Auger recombination processes involving valence bands that were forbidden in pure GaN became possible in InGaN.

The UCSB modelling team investigated the temperature dependence of the Auger recombination rate in InGaN – see Fig. 29 below. For the inter-band Auger process, which dominates in the visible spectrum, it was found that raising the temperature from 70 to 300 K resulted in a slight decrease in the magnitude of the rate, but also in a broadening of the "resonance", *i.e.* the range of energies over which the effect is important. **The magnitude of the calculated rate, on the order of 2 x 10^{30} cm^6/s, was consistent with this being an important loss mechanism in InGaN-based LEDs.**

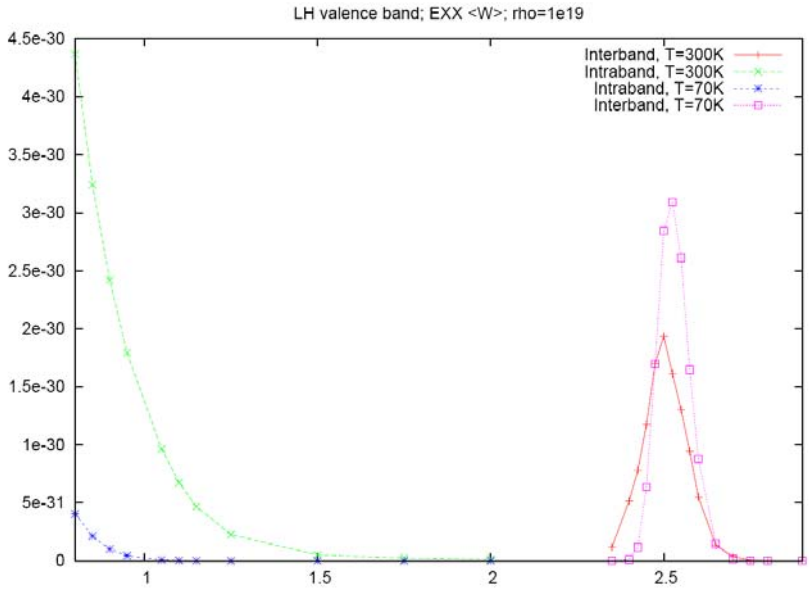

Fig. 29. Calculated Auger recombination rate in InGaN vs. band gap energy in electron volts.

For the intra-band Auger recombination process, they similarly found that raising the temperature led to a broadening of the energy range over which the effect is important; however, in this case they also found an increase in the magnitude of the effect. These intra-band processes would only occur for energies below 1.5 eV, *i.e.* outside the visible emission range.

In addition, UCSB continued its careful examinations of Auger matrix elements. They found that while at the Gamma point in the Brillouin zone only the crystal-field split-off band participates in the inter-band Auger process, away from this center all three valence bands contribute, although in slightly different proportions. This information may be of interest for quantum well structures, and was considered for additional study.

The importance of Auger recombination (in particular inter-conduction band recombination) as a loss mechanism in nitride-based light emitters has been mentioned above. An alternative loss process associated with the presence of a second conduction band at 2.5- 3.0 eV above the conduction band minimum is *inter*-conduction band absorption. To estimate the relevance of this process, Van de Walle *et al.* calculated the photon mean free path for the InGaN alloy model described above. The mean free path follows directly from the absorption coefficient, which was calculated by means of Fermi's golden rule with dipole matrix elements from first-principles

calculations. For typical device carrier densities of 10^{18} - 10^{19} cm^{-3}, the mean free path is of the order of 0.17 – 1.7 cm. Compared to the average mean free path in LEDs (30 nm) and laser diodes (300 μm), these results indicate that inter-conduction band absorption (ICBA) is probably not important for GaN-based light emitting diodes, but may potentially be relevant for laser devices. In actual devices, however, the lasing region consists of an InGaN quantum well and it is conceivable that quantum confinement effects could enhance ICBA. To get a more accurate estimate of ICBA in real devices, the team decided to use an infinite square well potential as an initial model for the InGaN quantum well.

In this framework, the confined electron wave functions are expressed in terms of the bulk InGaN Bloch states via a Fourier transform, and the dipole matrix elements between the InGaN quantum well states in terms of the dipole matrix elements between the corresponding bulk wave functions. The inter-conduction band absorption spectrum and photon mean free path are then calculated via Fermi's Golden Rule. The results at the end of the first year indicated that quantum confinement causes a shift of the absorption peak position and a slight increase in peak height. The calculated photon mean free path, however, was still large and the observed enhancement of ICBA was not significant enough to make ICBA a dominant loss mechanism in InGaN LEDs or laser diodes.

PRODUCTS OF PROJECT

Publications

During the project period one project-related publication was written, a pre-press draft of which was e-mailed to Program Manager Brian Dotson. The bibliographic reference for this peer-reviewed article is:

K.T. Delaney, P. Rinke, and C. Van de Walle, "Auger Recombination Rates in Nitrides from First Principles", Applied Physics Letters, 94, 191109 (2009).

Technologies/Techniques

The HVPE GaN growth techniques developed at Inlustra Technologies during the project period are of great value to its ongoing non-polar GaN substrate development efforts. Specifically, lateral epitaxial overgrowth methods were developed that provide a solid basis for uniform, wide-area reduction of GaN microstructural defect density. Such defects must be lowered to sufficient levels for high-yield GaN-based laser diode production, but in coming years ultra-high brightness LEDs driven at ever-higher currents will also require reduced defect density. Inlustra's mission is to develop scalable, economical methods for the production of GaN substrates using bulk growth techniques.